Nitrogen Stable Isotope Composition (δ^{15}N) of Vehicle-Emitted NO$_x$

Wendell W. Walters,*[,†] Stanford R. Goodwin,[‡] and Greg Michalski[†,‡]

[†]Department of Earth, Atmospheric, and Planetary Sciences and [‡]Department of Chemistry, Purdue University, 550 Stadium Mall Drive, West Lafayette, Indiana 47907, United States

Ⓢ Supporting Information

ABSTRACT: The nitrogen stable isotope ratio of NO$_x$ (δ^{15}N-NO$_x$) has been proposed as a regional indicator for NO$_x$ source partitioning; however, knowledge of δ^{15}N values from various NO$_x$ emission sources is limited. This study presents a detailed analysis of δ^{15}N-NO$_x$ emitted from vehicle exhaust, the largest source of anthropogenic NO$_x$. To accomplish this, NO$_x$ was collected from 26 different vehicles, including gasoline and diesel-powered engines, using a modification of a NO$_x$ collection method used by the United States Environmental Protection Agency, and δ^{15}N-NO$_x$ was analyzed. The vehicles sampled in this study emitted δ^{15}N-NO$_x$ values ranging from −19.1 to 9.8‰ that negatively correlated with the emitted NO$_x$ concentrations (8.5 to 286 ppm) and vehicle run time because of kinetic isotope fractionation effects associated with the catalytic reduction of NO$_x$. A model for determining the mass-weighted δ^{15}N-NO$_x$ from vehicle exhaust was constructed on the basis of average commute times, and the model estimates an average value of −2.5 ± 1.5‰, with slight regional variations. As technology improvements in catalytic converters reduce cold-start emissions in the future, it is likely to increase current δ^{15}N-NO$_x$ values emitted from vehicles.

INTRODUCTION

Nitrogen oxides (NO$_x$ = NO and NO$_2$) are important trace gases that affect atmospheric chemistry, air quality, and climate.[1] NO$_x$ play a key role in the troposphere by acting to control the concentrations of ozone (O$_3$) and the hydroxyl radical (OH) as well as forming nitrate (NO$_3^-$) aerosols.[2] The reactions between NO$_x$ and hydrocarbons (HC) are major sources of tropospheric O$_3$, which is a greenhouse gas, an oxidizing pollutant, and an influencer of the lifetimes of other greenhouse gases.[3−5] Ultimately, NO$_x$ is oxidized to nitric acid (HNO$_3$) and deposited as acid rain, leading to degradation of drinking water, soil acidification, lacustrine and estuarine eutrophication, and biodiversity changes in terrestrial ecosystems.[6]

Sources of NO$_x$ are both natural and anthropogenic, but there are uncertainties in the relative importance of these sources.[6−8] Natural sources of NO$_x$ include lightning, soil nitrification/denitrification, and wildfires.[6,8] Anthropogenic sources of NO$_x$ include fossil fuel and biofuel combustion (mainly emitted from power plants), transport (vehicles, ships, and aircraft), and industry.[7,8] Since the industrial revolution, anthropogenic emissions of NO$_x$ have surpassed natural NO$_x$ emissions.[6,7] Although significant improvements have been made to reduce NO$_x$ emissions from stationary and mobile sources, further progress is needed to reduce the health and ecosystems impacts associated with NO$_x$ emissions;[9] however, the uncertainty of total NO$_x$ emissions is relatively high, with an estimated uncertainty on the order of 30−50%.[6] To estimate the relative importance of various NO$_x$ sources and to assess the effectiveness of NO$_x$ reduction technologies, a way of partitioning NO$_x$ sources on the basis of nitrogen (N) deposition studies is required.

Once emitted into the atmosphere, NO$_x$ is primarily oxidized to HNO$_3$ and subsequently removed from the atmosphere via wet or dry deposition. Therefore, analysis of the N stable isotopes of atmosphere-derived nitrate (δ^{15}N-NO$_3^-$) could be used as a regional indicator for partitioning NO$_x$ sources, which would help identify the contribution of various NO$_x$ sources to local/regional N deposition as well as help evaluate the effectiveness of NO$_x$ emission reductions. Previous works have observed spatial variations in δ^{15}N-NO$_3^-$ in wet and dry deposition that correlated with the δ^{15}N-NO$_x$ of the surrounding areas stationary NO$_x$ emission sources (one-tailed, t test, $p < 0.001$), suggesting that δ^{15}N-NO$_3^-$ is linked to NO$_x$ sources.[10,11] Although the impact of kinetic and equilibrium isotopic fractionation of NO$_x$ sink processes (chemical reactions and photolysis) on δ^{15}N during the conversion of NO$_x$ to NO$_3^-$ must also be considered,[12,13] few fractionation factors for these sink processes have been determined. Previous measurements of δ^{15}N-NO$_x$ from various NO$_x$ sources are limited, but these indicate that NO$_x$ sources may have a wider range of δ^{15}N values than previously thought (Figure 1).[12,14−22] Although these prior measurements of δ^{15}N-NO$_x$ allow for an approximation of relative source contributions, further characterization of δ^{15}N-NO$_x$ is required to minimize
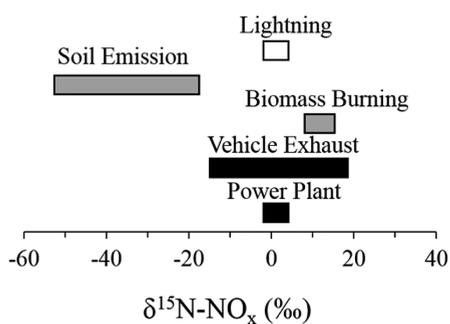
Figure 1. Range of $\delta^{15}N$ values for various NO_x sources.[12,14−22] Natural sources are indicated in white, anthropogenic sources are indicated in black, and a mixture of natural and anthropogenic sources are indicated in gray.

uncertainty in partitioning NO_x source contributions and to understand the impact of NO_x oxidation to HNO_3 on $\delta^{15}N$ values. Furthermore, it is possible that technology developments could influence the $\delta^{15}N\text{-}NO_x$ values of various NO_x sources, thus preventing the application of previous $\delta^{15}N\text{-}NO_x$ measurements to all regions.

In this study, the $\delta^{15}N\text{-}NO_x$ values of vehicle exhaust, the main source of anthropogenic emitted NO_x,[7] were measured. The source of N in vehicle exhaust is air with $\delta^{15}N = 0$‰; thus, it was previously assumed that NO_x formed by the oxidation of air would also have $\delta^{15}N$ near 0‰.[12,23] However, previous measurements of $\delta^{15}N\text{-}NO_x$ emitted directly from vehicle exhaust, indicate a rather large range of $\delta^{15}N\text{-}NO_x$, from −13 to 3‰.[12,14,16] Initial studies reported $\delta^{15}N\text{-}NO_x$ values of 3.7 and −1.8‰, supporting the assumption that $\delta^{15}N\text{-}NO_x$ emitted from vehicle exhaust is close to 0‰.[12,16] However, a subsequent study reported a much wider range of $\delta^{15}N\text{-}NO_x$ values, from −13 to −2‰, suggesting that $\delta^{15}N\text{-}NO_x$ from vehicle exhaust may not be as close to the previously assumed value of 0‰.[14] Recent studies of $\delta^{15}N\text{-}NO_x$ from vehicle exhaust have measured the $\delta^{15}N$ in plant material,[15,17,18] tree rings,[24] and/or the $\delta^{15}N$ from roadside NO_2[15,18,21] and indicate that vehicle-derived $\delta^{15}N\text{-}NO_x$ may have positive values as high as 17‰. Such inferences should be treated cautiously because they measure the $\delta^{15}N$ of a secondary product formed from vehicle-emitted NO_x that may be subject to kinetic and equilibrium isotope fractionation factors that can alter the initial $\delta^{15}N\text{-}NO_x$ value[12,13] and, in plant material $\delta^{15}N$ studies, because plant N requirements are likely not entirely derived from NO_x precursors. To characterize the $\delta^{15}N\text{-}NO_x$ emitted from modern vehicles, we measured in this study the $\delta^{15}N\text{-}NO_x$ directly emitted from vehicle exhaust for model years 1995 to 2015.

MATERIALS AND METHODS

NO_x Collection and Processing. NO_x was collected from the tailpipes of 26 different vehicles that included 15 passenger cars, 7 sports-utility vehicles (SUVs), and 4 trucks, using a modification of the United States Environmental Protection Agency (US EPA) Method 7 at West Lafayette, Indiana, USA (40.45° N, 86.91° W) between June 20, 2014 and September 26, 2014. The majority of exhaust samples were collected while vehicles were in neutral ($n = 22$), and a smaller set of exhaust samples were collected while vehicles were driven ($n = 4$); under both modes, the engine speed was kept between 2000 to 2500 rpm during sampling. Nineteen of the vehicles sampled had a "cold engine" (running less than 2 min prior to

sampling), and seven had a "warm engine" (running longer than 2 min prior to sampling). The model years of the sampled vehicles ranged from 1995 to 2015, and all vehicles had gasoline-powered engines except for one that had a diesel-powered engine. Every vehicle sampled was equipped with a 3-way catalytic converter. (For a complete list of sampled vehicles, see the Supporting Information.)

The sampling method used in this study was modified from US EPA Method 7 (Determination of Nitrogen Oxide Emissions from Stationary Sources). Briefly, exhaust samples were collected into evacuated 2 L borosilicate bottles. The 2 L bottles were connected to a Teflon tube (length of 35 cm and an inlet diameter of 1 cm) attached to a borosilicate probe with a length of 20 cm and an inlet diameter of 0.5 cm. The probe was placed into the tailpipes of each vehicle, and the stopcock to the borosilicate bottle was opened, allowing the exhaust to be collected. After a sampling period of approximately 10 s, the stopcock was closed. Because in the limiting case, the diameter of the sampling apparatus (0.5 cm) is approximately 73 500 times larger than the molecular mean-free path at ambient pressures (68 nm),[25] and the sampling time is approximately 1520 times quicker than the lifetime of NO diffusion through air ($\tau_{diff} = L^2/D \approx 15216.3$ s, where L = length of diffusion and D is the diffusion constant = 0.1988 cm^2/s)[26] for the total sampling apparatus length of 55 cm, diffusion isotope effects are negligible in this setup. Additionally, the estimated volume of the Teflon tube and the borosilicate probe was 30 mL, making the volume of sampled air in the probe negligible compared to that of the collected exhaust. The sampling bottles contained 10 mL of a NO_x absorbing solution, which was synthesized by mixing 2.8 mL of concentrated sulfuric acid (H_2SO_4) with 0.6 mL of 30% hydrogen peroxide (H_2O_2) that was diluted to 1 L using high-purity Millipore water. The absorbing solution quantitatively oxidizes NO_x into NO_3^-. Triplicate samples were collected for each vehicle, approximately 30 s apart.

After NO_x exhaust collection, the containers were allowed to stand for at least 72 h with occasional shaking every 10 to 12 h to facilitate the conversion of NO_x to NO_3^-. The residual NO_x headspace concentration was then measured using a Thermo Environmental Instrument Chemiluminescence NO-NO_2−NO_x Analyzer. The absorbing solution was collected and neutralized using 1 mL of 1 M sodium bicarbonate, and the NO_3^- concentration was measured using a Cary 5000 UV−vis spectrometer. Using the residual NO_x and NO_3^- concentrations, the percent of NO_x conversion to NO_3^- was calculated. Every sample had over 97.5% of the NO_x collected converted to NO_3^-; therefore, the N isotopic fractionation resulting from this conversion should be minimized. A potential interference that could impact the collected $\delta^{15}N\text{-}NO_3^-$ is the oxidation of ammonium (NH_4^+) to NO_3^-. Ammonia (NH_3) is known to be a major component of vehicle-emitted exhaust,[27] and once dissolved in the absorbing solution, it would presumably form NH_4^+. Because H_2O_2, a strong oxidizer, was a component of the absorbing solution, control tests were conducted to determine the possible conversion of NH_4^+ to NO_3^-. The results of the control tests indicated that in the absorbing solution used in this study no detectable NO_3^- formed from relatively high NH_4^+ concentrations (100 ppm). Therefore, NH_3 should have a minimal, if any, influence on the measured $\delta^{15}N\text{-}NO_3^-$. Overall, our control studies indicate that our absorbing solution and successive neutralization induces no N isotope fractionation.

Table 1. Vehicle Details and NO$_x$ Concentrations and δ^{15}N-NO$_x$ Values for Collected Exhaust Samples

year	make	model	$\bar{x}$-NO$_x$ (ppm)[a]	σ-NO$_x$ (ppm)[b]	$\bar{x}$-δ^{15}N (‰)[a]	σ-δ^{15}N (‰)[b]	n (replicates)	engine size (L)	engine temperature	mode
1995	Ford	Crown Victoria	72.3	15	−8.1	1.7	3	4.6	cold	driven
1996	Chevy	Suburban	101.1	35	−9.5	1.8	3	5.7	cold	neutral
2000	Chevy	Silverado	285.6	55	−10.3	1.9	3	4.8	cold	neutral
2000	Ford	Escort	31.2	13	−0.8	3.1	3	2.0	cold	neutral
2003	Chevy	Cavalier	55.2	80	0.3	5.4	3	2.2	cold	neutral
2003	Ford	Expedition	56.1	80	2.0	8.7	3	4.6	cold	neutral
2003	Honda	Accord	31.2	22	−0.4	1.5	3	2.4	warm	neutral
2003	Toyota	Corolla	23.1	4.5	−2.9	1.6	3	1.8	warm	neutral
2004	Ford	Taurus	121.2	150	−5.3	6.5	3	3.0	cold	neutral
2005	Dodge	Dakota	36.5	40	−3.6	7.9	3	3.7	cold	neutral
2005	Ford	Escape	138.9	10	−8.3	1.1	3	3.0	cold	neutral
2005	Pontiac	Trans Am	15.7	4	−0.4	1.8	3	3.6	warm	driven
2006	Kia	Spectra	22.7	13	0.6	3.0	3	3.4	cold	neutral
2006	Toyota	Highlander	9.9	0.2	8.6	1.6	3	2.0	wann	driven
2006	Volkswagen	GTI	30.1	6	−4.6	3.5	3	2.0	cold	neutral
2008	Ford	Fusion	21.3	10	1.6	4.0	3	2.4	warm	neutral
2008	Pontiac	G6	81.4	120	3.4	4.1	3	2.3	cold	neutral
2009	Mazda	CX-7	106.6	70	−9.6	4.3	3	2.3	cold	neutral
2009	Pontiac	Vibe	206.2	250	−9.0	5.3	3	1.8	cold	neutral
2010	GMC	Sierra Diesel	48.3	30	−19.1	3.8	3	6.0	cold	neutral
2011	Hyundai	Genesis	138.7	160	−4.4	6.2	3	2.0	cold	driven
2013	Kia	Sorento	20.9	10	2.4	6.7	3	2.4	cold	neutral
2014	Dodge	Ram	197.9	45	−12.2	0.4	3	5.7	cold	neutral
2014	Hyundai	Sonata Hybrid	8.8	0.9	9.8	1.1	3	2.4	warm	neutral
2014	Jeep	Cheroke	44.5	4	−5.5	0.8	3	2.1	cold	neutral
2015	Chevy	Suburban	8.5	0.5	1.6	1.1	3	5.3	warm	neutral

[a]$\bar{x}$ = mean. [b]σ = standard deviation.

Isotopic Analysis. For N isotopic analysis, approximately 250 nmol of NO$_3^-$ was injected into a 12 mL vial containing 1 mL of a denitrifying strain of bacteria (*P. aureofaciens*) that converts NO$_3^-$ to nitrous oxide (N$_2$O).[28] The N$_2$O was extracted and purified using an automated head-space gas chromatography system and analyzed for δ^{15}N values by a Thermo Delta V continuous-flow isotope ratio mass spectrometer (CF-IRMS) at the Purdue Stable Isotopes lab.[29] Values of δ^{15}N are reported in parts per thousand relative to atmospheric N$_2$, represented as

$$\delta^{15}N_{sample}\ (‰) = \frac{(^{15}N/^{14}N)_{sample} - (^{15}N/^{14}N)_{air}}{(^{15}N/^{14}N)_{air}} \times 1000$$

(1)

Working lab standards calibrated to NIST isotope reference nitrates USGS34 and USGS35 were used to correct for isotopic fractionation resulting from the denitrification of NO$_3^-$ and the subsequent N$_2$O purification process. The working standards had an average standard deviation of 0.3‰ for δ^{15}N.

RESULTS AND DISCUSSION

Table 1 details the vehicle information and the data measured from the vehicles sampled in this study. The text below summarizes the NO$_x$ concentrations and δ^{15}N-NO$_x$ values of the collected samples and discusses our interpretation of these results.

NO$_x$ Exhaust Concentration. The average concentration of NO$_x$ for individual vehicles ranged from 8.5 to 286 ppm, with standard deviations ranging from 0.2 to 250 ppm for triplicate samples. The large range and variance of emitted NO$_x$

can be explained by the run times of the engine prior to sampling that were divided into either cold engines (running less than 2 min prior to sampling) or warm engines (running longer than 2 min prior to sampling). Vehicles with cold engines emitted significantly more NO$_x$ (95 ± 70 ppm, n = 19) compared to warm engines (17 ± 8.6 ppm, n = 7), a finding that was statistically significant at a confidence level of 0.01 (p < 0.01). In the case of vehicles with cold engines, the highest NO$_x$ concentrations were always collected from the first sample, and NO$_x$ concentrations drastically decreased for subsequent samples. Alternatively, warm-engine vehicles generally emitted NO$_x$ at a consistent concentration for all samples collected. Overall, emitted NO$_x$ concentrations exhibited an exponential decay that moderately correlated with the vehicle run time prior to sampling for all samples (Figure 2).

These results are consistent with other studies that have shown that cold engines have higher emissions of NO$_x$.[30−33] This occurs because of a rich air−fuel ratio in cold engines and is due to the inefficiency of the 3-way catalytic converters at reducing NO$_x$ emissions under cold-engine conditions.[30−33] Generally, when an engine is first started, the fuel does not completely vaporize, and this causes higher emissions of hydrocarbons (HC), NO$_x$, and carbon monoxide (CO). As the engine reaches its operating temperature, the air−fuel ratio reaches the stoichiometric point for combustion, and catalytic converters become efficient, and the emissions of HC, CO, and NO$_x$ diminish.[30,33] Despite the progress made at reducing HC, CO, and NO$_x$ emissions with the 3-way catalytic converter, vehicles account for roughly 50% of the emissions of these gases,[32,34] with approximately 60−80% of the total emissions

$$y = 343.75e^{\left(-\frac{t}{31.62}\right)} + 14.99$$
$$R^2 = 0.451$$
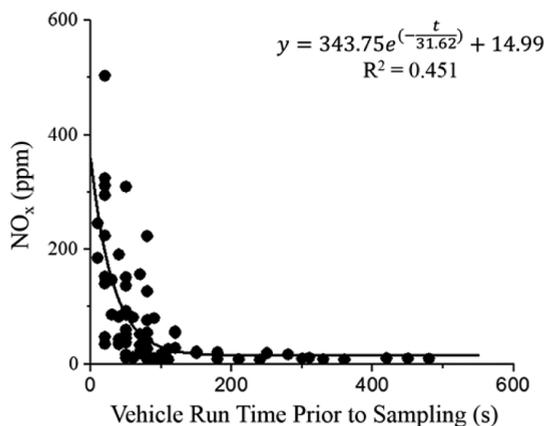
Figure 2. Emitted NO_x concentration as a function of vehicle run-time prior to sampling, represented as black circles, that is fit with an exponential decay represented by a solid line.

for a typical vehicle occurring during the first 200 s of cold-start operation, on the basis of the New European Driving Cycle.[35]

$\delta^{15}N\text{-}NO_x$ **Values.** The average $\delta^{15}N\text{-}NO_x$ measured for each vehicle ranged from −19.1 to 9.8‰, and the standard deviation ranged from 0.4 to 8.7‰ for triplicate samples. For most cases, the reported standard deviation was much greater than the analytical uncertainty of ±0.3‰. This large $\delta^{15}N\text{-}NO_x$ variance can be explained in terms of the emitted NO_x concentration. A strong, negative logarithmic correlation is observed between $\delta^{15}N\text{-}NO_x$ values and NO_x concentrations for gasoline- ($R^2 = 0.84$) and diesel-powered engines ($R^2 = 0.98$) (Figure 3). There was no significant difference between

$$y = -5.16(\pm 0.3)x + 15.95(\pm 1)$$
$$R^2 = 0.84$$

$$y = -6.13(\pm 0.8)x + 3.93(\pm 3)$$
$$R^2 = 0.98$$
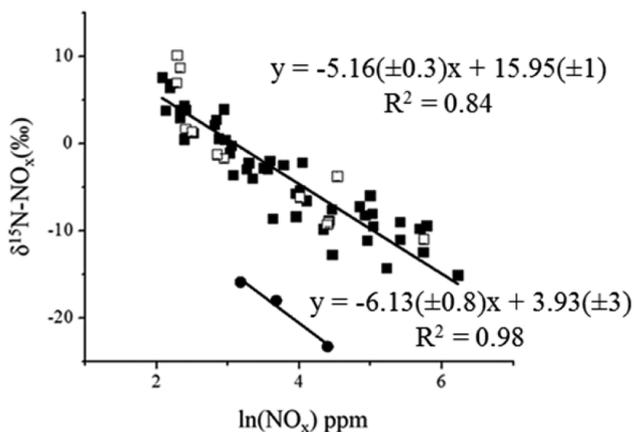
Figure 3. $\delta^{15}N\text{-}NO_x$ (‰) as a function of collected $\ln(NO_x)$ (ppm), where black data points represent samples collected from vehicles while in neutral and white data points represent exhaust samples collected from vehicles while driven. Square points represent gasoline-powered engines, and circle points represent diesel-powered engines.

vehicles sampled while in neutral or while driven because both modes resulted in $\delta^{15}N\text{-}NO_x$ that similarly correlated with emitted NO_x concentration (Figure 3). The measured $\delta^{15}N\text{-}NO_x$ values are hypothesized to have arisen from the thermal production of NO_x in the combustion chamber that would result in NO_x depleted in ^{15}N and from the subsequent equilibrium isotope effects and the catalytic reduction of NO_x to N_2 that would enrich ^{15}N relative to the thermally produced NO_x. This hypothesis was tested using theoretical isotope-fractionation factors in kinetic and Rayleigh distillation models.

Thermal Production of NO. The most well-known chemical pathway for the formation of NO_x in internal combustion engines is the Zeldovich mechanism,[36] in which NO is formed by the reaction between nitrogen and oxygen in the intake air, represented as

$$N_2 + O \rightarrow NO + O \tag{R1}$$

$$N + O_2 \rightarrow NO + O \tag{R2}$$

$$N + OH \rightarrow NO + H \tag{R3}$$
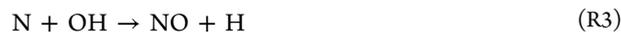
Under temperatures of the thermal production of NO ($T > 2000$ K), it has been previously assumed that N_2, O_2, and NO exist at isotopic equilibrium, represented as[12,23]

$$N_2 + O_2 \leftrightarrow 2NO \tag{R4}$$

The calculated equilibrium exchange fractionation factor for this reaction is extremely small (<1.69‰);[37] therefore, the thermally produced NO should have a $\delta^{15}N$ value close to that of air (0‰). However, the majority of our measured NO_x was depleted in ^{15}N, especially for cold-engine vehicles. This suggests that the thermal production of NO in a combustion chamber in a vehicle engine is not always achieving equilibrium, and its formation is kinetically limited by the large amount of energy required to break the triple bond of N_2 (R1).

A previous study that measured depleted ^{15}N abundances in vehicle exhaust NO_x attributed the ^{15}N depletion to the kinetic isotope effect associated with the breaking of the triple bond of N_2.[14] Because of the difference in zero-point energies (ZPE), this bond breaking is faster for the lighter isotopologues ($^{14}N^{14}N$, ZPE = 1175.7 cm^{-1})[38] relative to the heavier isotopologue ($^{15}N^{14}N$, ZPE = 1156.0 cm^{-1}).[38] If the difference between N_2 bond dissociation for $^{14}N^{14}N$ molecule and $^{15}N^{14}N$ molecule is significant at combustion temperatures, then the thermally produced NO will tend to have $\delta^{15}N$ values lower than those of atmospheric N_2. To quantify this kinetic isotope effect, so as to understand its impact on $\delta^{15}N\text{-}NO_x$, the kinetics of the thermal production of NO_x were simulated using *Kintecus*, a kinetics compiler that can be used to model chemical kinetic processes.[39] Table 2 summarizes the reactions included in this model and the corresponding Arrhenius rate parameters.[40−43] Rate constants for the molecules involving ^{14}N were taken from the NIST Chemical Kinetics Database.[44] These rate constants were adjusted for ^{15}N by calculating the relative reaction rates and, therefore the fractionation factors (α), of the heavy isotope to the light isotope from the inverse of the reduced masses (μ) of the activated complex at the transition state (eq 2), subsequently scaling the reaction rate of the light isotope for the heavier isotope (eq 3).

$$\alpha_{H/L} = \frac{k_H}{k_L} = \sqrt{\frac{\mu_L^{\ddagger}}{\mu_H^{\ddagger}}} \tag{2}$$

$$k(T)_{heavy} = \alpha_{H/L} A \left(\frac{T}{298}\right)^n e^{(-E_a/RT)} \tag{3}$$

In eq 2, k is the reaction rate, $\mu^{\ddagger}$ is the reduced mass of the activated complex, H represents the heavier N isotopologue (^{15}N), and L represents the lighter N isotopologue (^{14}N). In eq 3, A is the Arrhenius pre-exponential factor, T is temperature (in degrees Kelvin), n is the temperature dependence, E_a is the activation energy, and R is the gas constant. Kinetic isotope effects are caused by differences in the activation energy for

Table 2. Data for the Reactions and the Rate Constants for the Thermal Production of NO[40−43,a]

	reaction	α	A	n	E_a (kJ/mol)
1	$^{14}N_2 \rightarrow 2\,^{14}N$	1	9.86×10^{-05}	-3.33	940
	$^{15}N^{14}N \rightarrow\ ^{14}N +\ ^{15}N$	0.983	9.86×10^{-05}	-3.33	940
2	$O_2 \rightarrow 2O$		1.01×10^{-08}	-1	494
3	$^{14}N_2 + O \rightarrow\ ^{14}NO +\ ^{14}N$	1	3.01×10^{-10}	0	318
	$^{15}N^{14}N + O \rightarrow\ ^{14}NO +\ ^{15}N$	0.997	1.51×10^{-10}	0	318
	$^{15}N^{14}N + O \rightarrow\ ^{15}NO +\ ^{14}N$	0.995	1.51×10^{-10}	0	318
4	$^{14}N + O_2 \rightarrow\ ^{14}NO + O$	1	4.47×10^{-12}	1	27.19
	$^{15}N + O_2 \rightarrow\ ^{15}NO + O$	0.994	4.47×10^{-12}	1	27.19
5	$^{14}N + OH \rightarrow\ ^{14}NO + H$	1	4.70×10^{-08}	0	-0.71
	$^{15}N + OH \rightarrow\ ^{15}NO + H$	0.999	4.70×10^{-08}	0	-0.71

[a] $k(T) = \alpha A (T/298)^n e^{(-E_a/RT)}$, and α represents the relative reaction rate for the N isotopologues.

reactions involving different isotopes because of the transition state having different zero-point vibrational energies. Vibrational frequencies (ω_e), and thus vibrational zero-point energies, depend on the reduced mass (μ) of the vibrating system, represented as

$$\omega_e = \frac{1}{2\pi}\sqrt{\frac{k}{\mu}} \tag{4}$$

where k is the bond force constant. The ground vibrational mode ($1/2h\omega_e$), where h is planck's constant, is inversely proportional to the square root of the reduced mass ($\mu^{1/2}$). Therefore, the inverse of the reduced mass of the activated complex is an adequate approximation for the kinetic isotope effect associated with chemical reactions. For this approximation to be valid at high temperatures, the population of the ground vibrational modes needs to be considered. Both N_2 and NO have relatively high-energy vibrational modes of 2359 and 1904 cm^{-1}, respectively, associated with vibrational stretching modes.[45] The population of molecules in the ground vibrational state can be calculated on the basis of the Boltzmann distribution and the harmonic oscillator approximation, represented as

$$f_i = (1 - e^{(-h\nu/kT)}) \tag{5}$$

where h is Plank's constant, ν is the vibrational frequency, k is Boltzmann constant, and T is temperature. At typical combustion temperatures (~2000 K), the majority of N_2 (81.7%) and NO (73.3%) exist in the ground vibrational state. Therefore, this harmonic oscillator approximation of the activated complexes will be an adequate approximation for this system.

Our $\delta^{15}N$ thermal NO production model is an approximation; however, the model suggests that the thermal production of NO will result in a $\delta^{15}N$ value of $-9.5‰$, assuming that the source of N is air that has $\delta^{15}N = 0‰$. This value is in excellent agreement with the $\delta^{15}N$-NO$_x$ values previously measured (-11 to $-7‰$) for gasoline-powered vehicle exhaust associated with the kinetically limited thermal production of NO.[14] Presumably, this is the lowest $\delta^{15}N$-NO$_x$ value emitted from vehicles because subsequent equilibrium isotope effect between N_2 and NO (R4)[14] and the catalytic reduction of NO$_x$ would increase the $\delta^{15}N$-NO$_x$ value. However, diesel-powered vehicles seem to have slightly lower

$\delta^{15}N$-NO$_x$ values than what our thermal production of NO$_x$ model predicts. The NO$_x$ samples from diesel-powered vehicles analyzed in this study had $\delta^{15}N$-NO$_x$ values that ranged from -23.3 to $-15.9‰$, and in a previous study, measured $\delta^{15}N$-NO$_x$ values ranged from -13 to $-12‰$ for the kinetically limited thermal production of NO$_x$.[14] These lower $\delta^{15}N$-NO$_x$ values likely occur because of the different combustion conditions in diesel vehicles compared to those in gasoline-powered vehicles.[46] Diesel-powered vehicles primarily operate at lower combustion temperatures than gasoline-powered vehicles.[46] This is likely to increase N isotope fractionation and result in lower $\delta^{15}N$-NO$_x$ values from the thermal production of NO$_x$ compared to those from gasoline-powered engines. Although the exact $\delta^{15}N$-NO$_x$ produced from combustion is difficult to predict because of the variability in combustion conditions,[46] the kinetically limited thermal NO$_x$ production should result in negative $\delta^{15}N$ values.

Catalytic Reduction of NO. Another kinetic isotope effect to consider is that from the reaction of NO$_x$ with a 3-way catalytic converter. A 3-way catalytic converter uses a metal catalyst, typically platinum and rhodium, to reduce NO$_x$ emissions upward of 90%.[47] The catalytic reduction of NO$_x$ to N_2 can be described as NO decomposition on the catalyst surface followed by the removal of the oxygen on the catalyst surface through a reaction with a reducing agent such as carbon monoxide (CO).[47] Infrared studies of NO adsorption on aluminum- and silica-supported rhodium have provided evidence for stable molecular adsorption of NO on rhodium,[48−50] and temperature-programmed desorption studies have provided evidence for the dissociation of NO on rhodium to form N and O.[51−54] For NO to be reduced to N_2, it has to first undergo adsorption onto the metal catalyst surface. For this process to occur, NO$_x$ has to diffuse through a washcoat layer approximately 10−50 μm thick and then bind onto the catalyst surface,[34,55] likely leading to isotopic fractionation. The lighter molecules (^{14}NO) will diffuse through the washcoat diffusion layer of the catalyst and undergo adsorption more quickly onto the catalyst surface than the heavier molecules (^{15}NO) because of differences in mass and zero-point energies, respectively. This will cause the lighter NO molecules to preferentially decompose to their elemental components with the heavier NO molecules to be emitted when the catalytic converter is effectively operating, thus causing the emitted NO$_x$ to be enriched in ^{15}N relative to the

thermally produced NO. The number of potentially fractionating reactions and difficulties in assessing catalytic isotope effects for each step is beyond the scope of this work. Rather, the observed $\delta^{15}N\text{-}NO_x$ and NO_x concentration were used in a Rayleigh distillation model to determine the catalytic converter's net isotope effect, which includes diffusion, equilibrium, and kinetic effects.

$\delta^{15}N\text{-}NO_x$ Exhaust Fractionation Factor. The results of this study indicate a strong relationship between the emitted NO_x concentration and $\delta^{15}N\text{-}NO_x$ (Figure 3): in general, the more concentrated the NO_x emission, the lower the $\delta^{15}N\text{-}NO_x$ value. Our kinetics model indicates that thermally produced NO is depleted in ^{15}N. In the absence of a 3-way catalytic converter or under conditions of inefficient NO_x reduction (cold engine and catalytic converter), the kinetically limited NO_x production is likely to result in a negative $\delta^{15}N\text{-}NO_x$ value. As the vehicle engine becomes more efficient and the catalytic converter warms up, NO_x emissions are reduced, and the NO_x becomes enriched in ^{15}N relative to thermally produced NO, likely as a result of the equilibrium isotope effect between N_2 and NO (R4)[14] as well as the kinetic isotope effect associated with the diffusion and adsorption of NO_x onto the catalytic converter surface as previously discussed.

To quantitatively determine the $\delta^{15}N$ isotope fractionation associated with the reduction of NO_x caused by the warming of a vehicle engine and catalytic converter, this process was modeled according to a Rayleigh type fractionation, represented as.

$$\delta^{15}N_f = \delta^{15}N_o - \varepsilon \ln[NO_x] \qquad (6)$$

where $\delta^{15}N_f$ is the measured $\delta^{15}N\text{-}NO_x$, $\delta^{15}N_o$ is $\delta^{15}N\text{-}NO_x$ value that vehicle-emitted NO_x reaches as NO_x emissions approach zero, and ε is the enrichment factor for $\delta^{15}N$ as the concentration of NO_x decreases. The enrichment factor (ε) is related to the fractionation factor (α) of the reduction of NO_x by the relationship represented as

$$\varepsilon \ (‰) = (\alpha - 1) \times 1000 \qquad (7)$$

From Figure 3, the enrichment factor (ε) for the production of vehicle-emitted NO_x was calculated for gasoline- and diesel-powered engines to be $5.2(\pm0.3)‰$ and $6.13(\pm0.8)‰$, respectively. This indicates that as the engine and catalytic converter warm up, the lighter molecules of NO_x are preferentially decomposed, leaving the emitted NO_x enriched in ^{15}N compared to atmospheric air. This suggests that vehicle-emitted NO_x has likely become enriched in the ^{15}N isotope relative to the vehicle-emitted NO_x produced prior to 1975 because of the advent of the 3-way catalytic converter.

Implications for $\delta^{15}N\text{-}NO_x$. The data obtained from this study are limited and do not represent the $\delta^{15}N\text{-}NO_x$ emitted from all types of vehicles, but they are useful for $\delta^{15}N\text{-}NO_x$ source characterization of vehicle exhaust. In this study, we measured a rather large range of $\delta^{15}N\text{-}NO_x$ for individual samples, ranging from -15.1 to $10.5‰$ for gasoline-powered vehicles and -23.3 to $-15.9‰$ for diesel-powered vehicles. In general, the lowest $\delta^{15}N\text{-}NO_x$ values came from cold-start vehicles that were emitting high concentrations of NO_x. As previously mentioned, approximately $60-80\%$ of the total emissions for a typical vehicle occur during the first 200 s of cold-start operation.[35] Therefore, in order to estimate the mass-weighted $\delta^{15}N\text{-}NO_x$ emitted from vehicles, the mass balance of the emitted NO_x concentration needs to be accounted for. To

this end, a model was constructed on the basis of numerical integration methods to relate the concentration of emitted NO_x (Figure 2) as a function of vehicle run time with the instantaneous vehicle-emitted $\delta^{15}N\text{-}NO_x$ for gasoline-powered vehicles. Specific details on the construction of this model can be found in the Supporting Information. This model predicts the mass-weighted $\delta^{15}N\text{-}NO_x$ emitted from vehicles to have the following relationship with vehicle run time represented as

$$y = -12.35 + 3.02 \ln(t + 0.455) \qquad (8)$$

where y is the mass-weighted $\delta^{15}N\text{-}NO_x (‰)$ emitted from vehicles and t is vehicle run time (min). This model shows the importance of NO_x mass-balance to the overall $\delta^{15}N\text{-}NO_x$. Because NO_x emissions are highest and are lowest in ^{15}N during the cold-start period, this will lower the overall emitted $\delta^{15}N\text{-}NO_x$ from vehicles. A similar type of analysis was not carried out for diesel-powered engines because of the small sample size measured in this study ($n = 3$).

The average commute time varies regionally in the USA,[56] and this likely leads to slight differences in the emitted $\delta^{15}N\text{-}NO_x$ from vehicle exhaust. The United States Census Bureau American Community Survey's zip code one-way commute time inventory[56] was used with the $\delta^{15}N\text{-}NO_x$ cumulative release time function (eq 8), to estimate the $\delta^{15}N\text{-}NO_x$ of vehicle exhaust emissions in each zip code in the continental USA (Figure 4). Overall, the average one-way commute time in
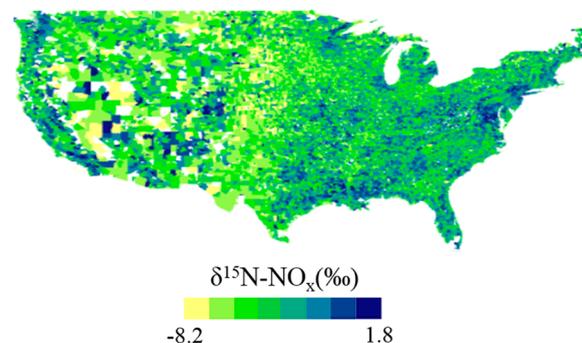
Figure 4. Regional variation in commute time and the resulting predicted $\delta^{15}N\text{-}NO_x$ from vehicle exhaust. White regions represent areas that did not have reported average commute time data.[56]

the United States is approximately 25.4 min,[56] corresponding with a $\delta^{15}N\text{-}NO_x$ value of $-2.5 \pm 1.5‰$. Although this average commute time represents all modes of transportation, the majority of transportation is from vehicles (86.1%), so this should be an adequate estimate for the regional $\delta^{15}N\text{-}NO_x$ emitted from vehicle exhaust.[56] This $\delta^{15}N\text{-}NO_x$ approximation only accounts for gasoline-powered engines. Our few measurements of diesel-powered engines had lower $\delta^{15}N\text{-}NO_x$ values than those of gasoline-powered engines. Therefore, if these measurements are representative of all diesel-powered engines, inclusion of diesel-powered engines to the overall mass-weighted $\delta^{15}N\text{-}NO_x$ would lead to a lower $\delta^{15}N\text{-}NO_x$ value. However, the percentage of diesel-powered passenger vehicles in the U.S. is roughly 2.8%,[57] so the impact of diesel-powered vehicles on the mass-weighted $\delta^{15}N\text{-}NO_x$ from passenger vehicle exhaust is likely to be small.

Several studies have measured the $\delta^{15}N\text{-}NO_3^-$ in wet[10,12,58] and dry deposition,[11] and these values range from -9.5 to $14.1‰$, outside of the mass-weighted $\delta^{15}N\text{-}NO_x$ value of vehicle-emitted NO_x. Additionally, a recent highway-tunnel

δ^{15}N-NO$_2$ study measured δ^{15}N values that ranged from 10.2 to 17‰,[21] which is higher than the majority of the δ^{15}N-NO$_x$ measurements made in this study. This discrepancy in δ^{15}N-NO$_x$ of vehicle-emitted NO$_x$ and of δ^{15}N-NO$_3^-$ deposition and δ^{15}N-NO$_2$ roadside studies are likely explained either by equilibrium[13] and/or kinetic isotope effects[12] that slightly alter the δ^{15}N of the original NO$_x$ source or by the contribution of other NO$_x$ sources with different δ^{15}N-NO$_x$ values (Figure 1). The exact causation of the alteration of δ^{15}N is beyond the scope of this work; however, if the δ^{15}N of atmospheric NO$_3^-$ is controlled by the source δ^{15}N-NO$_x$, then Figure 4 suggests that (1) there will be spatial variations in the δ^{15}N of NO$_3^-$ tied to commute time and vehicle NO$_x$ mitigation efficiency, (2) there would be temporal variations in δ^{15}N of NO$_3^-$ related to the transition from nonvehicle to vehicle NO$_x$ production during the day and week, and (3) the δ^{15}N of atmospheric NO$_3^-$ produced between 1950 and 1975 should be significantly lower relative to NO$_3^-$ produced after 1980, which should be detectable in the northern hemisphere ice core record.[19,59]

The continual improvements of the 3-way catalytic converter will likely have a future impact on δ^{15}N-NO$_x$ values. Once catalytic converters are warmed up, they are up to 97% effective at reducing toxic gas emissions.[47,60] However, these high conversion rates are only achieved when the converter is at a temperature of (typically) 300 °C or greater, which can take several minutes to achieve.[60] This results in more than 60−80% of total emissions occurring during cold-start emissions.[61] Decreasing these cold-start emissions is the objective of future catalytic converter improvements.[62] As these technological advancements become commonplace for catalytic-converter-equipped vehicles, it will likely lead to an increase of the δ^{15}N-NO$_x$ value relative to the current value because of the fractionation factor associated with the catalytic reduction of NO$_x$.

■ ASSOCIATED CONTENT

ⓢ Supporting Information

Appendix table and mass-weighted δ^{15}N-NO$_x$ emission model. This material is available free of charge via the Internet at http://pubs.acs.org.

■ AUTHOR INFORMATION

Corresponding Author

* E-mail: waltersw@purdue.edu. Phone: (765)-496-4906. Fax: (765)-496-1210.

Notes

The authors declare no competing financial interest.

■ REFERENCES

(1) Solomon, S., Qin, D., Manning, M., Chen, Z., Marquis, M., Averyt, K. B., Tignor, M., Miller, H. L., Eds. *Climate change 2007: The physical science basis: contribution of Working Group I to the Fourth Assessment Report of the Intergovernmental Panel on Climate Change*; Cambridge University Press: New York, 2007.

(2) Lawrence, M. G.; Crutzen, P. J. Influence of NO$_x$ emissions from ships on tropospheric photochemistry and climate. *Nature* **1999**, *402*, 167−170.

(3) Crutzen, P. J. The role of NO and NO$_2$ in the chemistry of the troposphere and stratosphere. *Annu. Rev. Earth Planet. Sci.* **1979**, *7*, 443−472.

(4) Atkinson, R. Atmospheric chemistry of VOCs and NO$_x$. *Atmos. Environ.* **2000**, *34*, 2063−2101.

(5) Atkinson, R.; Arey, J. Gas-phase tropospheric chemistry of biogenic volatile organic compounds: A review. *Atmos. Environ.* **2003**, *37*, 197−219.

(6) Galloway, J. N.; Dentener, F.; Capone, D.; Cleveland, C.; Green, P.; Holland, E.; Karl, D.; Michaels, A.; Porter, J.; Townsend, A.; Vorosmarty, C. Nitrogen cycles: past, present, and future. *Biogeochemistry* **2004**, *70*, 153−226.

(7) Reis, S.; Pinder, R. W.; Zhang, M.; Lijie, G.; Sutton, M. A. Reactive nitrogen in atmospheric emission inventories. *Atmos. Chem. Phys.* **2009**, *9*, 7657−7677.

(8) Jaeglé, L.; Steinberger, L.; Martin, R. V.; Chance, K. Global partitioning of NO$_x$ sources using satellite observations: Relative roles of fossil fuel combustion, biomass burning and soil emissions. *Faraday Discuss.* **2005**, *130*, 407−423.

(9) Melillo, J. M.; Cowling, E. B. Reactive Nitrogen and Public Policies for Environmental Protection. *Ambio* **2002**, *31*, 150−158.

(10) Elliott, E. M.; Kendall, C.; Wankel, S. D.; Burns, D. A.; Boyer, E. W.; Harlin, K.; Bain, D. J.; Butler, T. J. Nitrogen isotopes as indicators of NO$_x$ source contributions to atmospheric nitrate deposition across the Midwestern and Northeastern United States. *Environ. Sci. Technol.* **2007**, *41*, 7661−7667.

(11) Elliott, E. M.; Kendall, C.; Boyer, E. W.; Burns, D. A.; Lear, G.; Golden, H. E.; Harlin, K.; Bytnerowicz, A.; Butler, T. J.; Glatz, R. Dual nitrate isotopes in actively and passively collected dry deposition: Utility for portioning NO$_x$ sources, understanding reaction pathways, and comparison with isotopes in wet nitrate deposition. *J. Geophys. Res.: Biogeosci.* **2009**, *114*, G04020.

(12) Freyer, H. D. Seasonal trends of NH$_4^+$ and NO$_3^-$ nitrogen isotope composition in rain collected in Julich, West Germany. *Tellus* **1978**, *30*, 83−92.

(13) Freyer, H. D.; Kley, D.; Volz-Thomas, A.; Kobel, K. On the interaction of isotopic exchange processes with photochemical reactions in atmospheric oxides of nitrogen. *J. Geophys. Res.: Atmos.* **1993**, *98*, 14791−14796.

(14) Heaton, T. H. E. ^{15}N/^{14}N ratios of NO$_x$ from vehicle engines and coal-fired power 770 stations. *Tellus* **1990**, *42B*, 304−307.

(15) Ammann, M.; Siegwolf, R.; Pichlmayer, F.; Suter, M.; Brunold, C. Estimating the uptake of traffic-derived NO$_2$ from ^{15}N abundance in Norway spruce needles. *Oecologia* **1999**, *188*, 124−131.

(16) Moore, H. The isotopic composition of ammonia, nitrogen dioxide, and nitrate in the atmosphere. *Atmos. Environ.* **1977**, *11*, 1230−1243.

(17) Pearson, J.; Wells, D.; Seller, K.; Bennett, A.; Soares, A.; Woodall, J.; Ingrouille, M. Traffic exposure increases natural ^{15}N and heavy metal concentrations in mosses. *New Phtol.* **2000**, *147*, 317−326.

(18) Redling, K.; Elliott, E.; Bain, D.; Sherwell, J. Highway contributions to reactive nitrogen deposition: tracing the fate of vehicular NOx using stable isotopes and plant biomonitors. *Biogeochemistry* **2013**, *116*, 261−274.

(19) Hastings, M. G.; Jarvis, J. C.; Steig, E. J. Anthropogenic impacts on nitrogen isotopes of ice-core nitrate. *Science* **2009**, *324*, 1288.

(20) Felix, J. D.; Elliot, E. M.; Shaw, S. L. Nitrogen isotopic composition of coal-fired power plant NO$_x$: influence of emission controls and implications for global emission inventories. *Environ. Sci. Technol.* **2012**, *46*, 3528−3535.

(21) Felix, J. D.; Elliott, E. M. Isotopic composition of passively collected nitrogen dioxide emissions: Vehicle, soil, and livestock source signatures. *Atmos. Environ.* **2014**, *92*, 359−366.

(22) Li, D.; Wang, X. Nitrogen isotopic signature of soil-released nitric oxide (NO) after fertilizer application. *Atmos. Environ.* **2008**, *42*, 4747−4754.

(23) Heaton, T. H. E. $^{15}N/^{14}N$ ratios of nitrate and ammonium in rain at Pretoria, South Africa. *Atmos. Environ.* **1987**, *21*, 843−852.

(24) Savard, M. M.; Begin, C.; Smirnoff, A. Tree-ring nitrogen isotopes reflect anthropogenic NO_x emissions and climatic effects. *Environ. Sci. Technol.* **2009**, *43*, 604−609.

(25) Jennings, S. G. The mean free path in air. *J. Aerosol Sci.* **1988**, *19*, 159−166.

(26) Massman, W. J. A review of the molecular diffusivities of H_2O, CO_2, CH_4, CO, O_3, SO_2, NH_3, N_2O, NO and NO_2 in air, O_2, and N_2 near STP. *Atmos. Environ.* **1998**, *32*, 1111−1127.

(27) Heeb, N. V.; Saxer, C. J.; Forss, A.; Bruhlmann, S. Trends of NO^-, NO_2^-, and NH_3^- emissions from gasoline-fueled Euro-3 to Euro-4 passenger cars. *Atmos. Environ.* **2008**, *42*, 2543−2554.

(28) Sigman, D. M.; Casciotti, K. L.; Andreani, M.; Barford, D.; Galanter, M.; Böhlke, J. K. A bacterial method for the nitrogen isotopic analysis of nitrate in seawater and freshwater. *Anal. Chem.* **2001**, *73*, 4145−4153.

(29) Crawley, L. R. Nitrogen and oxygen isotope-ratio analysis of nitrate by the denitrifier method using continuous flow isotope-ratio mass spectrometery. Masters Dissertation, Purdue University, West Lafayette, IN, 2010.

(30) Dunne, S. R.; Raymond A. R. Use of a molecular sieve bed to minimize emissions during cold start of internal combustion engines. U.S. Patent 5,051,244, September 24, 1991.

(31) Yang, B. L.; Harold, H. K. Reactor trap to remove hydrocarbons from engine exhaust during cold start. *Environ. Sci. Technol.* **1994**, *28*, 1561−1564.

(32) Leclerc, J. P.; Schweich, D. Modeling Catalytic Monoliths for Automobile Emission Control. In *Chemical Reactor Technology for Environmentally Safe Reactors and Products*. de Lasa, H. I., Dogu, G., Ravella, A., Eds.; Kluwer Academic Publishers: Dordrecht, The Netherlands, 1993; p 547.

(33) Pulkrabek, W. W. *Engineering fundamentals of the internal combustion engine*; Pearson Prentice Hall: Upper Saddle River, NJ, 2014.

(34) Hayes, R. E.; Mukadi, L. S.; Votsmeier, M.; Gieshoff, J. Three-way catalytic converter modelling with detailed kinetics and washcoat diffusion. *Top. Catal.* **2004**, *30*, 411−415.

(35) Koltsakis, G. C.; Stamatelos, A. M. Catalytic Automotive Exhaust Aftertreatment. *Prog. Energy Combust. Sci.* **1997**, *23*, 1−39.

(36) Zeldovich, J. The oxidation of nitrogen in combustion and explosions. *Acta Physiochim. URSS* **1946**, *11*, 577−628.

(37) Richet, P.; Bottinga, Y.; Janoy, M. A review of hydrogen, carbon, nitrogen, oxygen, sulphur, and chlorine stable isotope enrichment among gaseous molecules. *Annu. Rev. Earth Planet. Sci.* **1977**, *5*, 65−110.

(38) Huber, K. P.; Herzberg, G. *Molecular Spectra and Molecular Structure* Vol. IV. Constants of Diatomic Molecules; Van Nostrand Reinhold: New York, 1979.

(39) Ianni, J. C. *Kintecus*, Windows version 5.20, 2014. www.kintecus.com.

(40) Thielen, K.; Roth, P. N atom measurements in high-temperature N_2 dissociation kinetics. *AIAA J.* **1986**, *24*, 1102−1105.

(41) Tsang, W.; Hampson, R. F. Chemical kinetic data base for combustion chemistry. Part I. Methane and related compounds. *J. Phys. Chem. Ref. Data* **1986**, *15*, 1087−1279.

(42) Baulch, D. L.; Cobos, C. J.; Cox, R. A.; Frank, P.; Hayman, G.; Just, T.; Kerr, J. A.; Murrells, T.; Pilling, M. J.; Troe, J.; Walker, R. W.; Warnatz, J. Evaluated kinetic data for combustion modeling. Supplement I. *J. Phys. Chem. Ref. Data* **1994**, *23*, 847−848.

(43) Atkinson, R.; Baulch, D. L.; Cox, R. A.; Hampson, R. F.; Kerr, J. A.; Troe, J. Evaluated kinetic and photochemical data for atmospheric chemistry: Supplement III. IUPAC subcommittee on gas kinetic data evaluation for atmospheric chemistry. *J. Phys. Chem. Ref. Data* **1989**, *18*, 881−1097.

(44) Manion, J. A. ; Huie, R. E.; Levin, R. D.; Burgess, D. R.; Orkin, V. L.; Tsang, W.; McGivern, W. S.; Hudgens, J. W.; Knyazev, V. D.; Atkinson, D. B.; Chai, E.; Tereza, A. M.; Lin, C. Y.; Allison, T. C.; Mallard, W. G. ; Westley, F.; Herron, J. T.; Hampson, R. F.; and Frizzell, D. H. *NIST Chemical Kinetics Database, Standard Reference Database 17*, version 7.0 (web version, release 1.6.8, data version 2013.03); National Institute of Standards and Technology, Gaithersburg, MD. http://kinetics.nist.gov.

(45) Shimanouchi, T. *Tables of Molecular Vibrational Frequencies, Consolidated Volume 1*; National Standard Reference Data Series, National Bureau of Standards Publication 39; United States Department of Commerce: Washington, DC, 1972.

(46) Iserman, R. *Engine Modeling and Control: Modeling and electronic management of internal combustion engines*. Springer: New York, NY, 2014.

(47) Taylor, K. C. Nitric Oxide Catalysis in Automotive Exhaust Systems. *Catal. Rev.: Sci. Eng.* **1993**, *35*, 457−481.

(48) Arai, H.; Tominaga, H. An infrared study of nitric oxide on rhodium-alumina catalyst. *J. Catal.* **1976**, *43*, 131−142.

(49) Solymosi, F.; Sárkány, J. An infrared study of the surface interaction between NO and CO on Rh/Al_2O_3 catalyst. *Appl. Surf. Sci.* **1979**, *3*, 68−82.

(50) Hecker, W. C.; Bell, A. T. Reduction of NO by CO over silica-supported rhodium: Infrared and kinetic studies. *J. Catal.* **1983**, *84*, 200−215.

(51) Campbell, C. T.; White, J. M. Chemisorption and reactions of nitric oxide on rhodium. *Appl. Surf. Sci.* **1978**, *1*, 347−359.

(52) Chin, A. A.; Bell, A. T. Kinetics of nitric oxide decomposition on silica-supported rhodium. *J. Phys. Chem.* **1983**, *87*, 3700−3706.

(53) Baird, R. J.; Ku, R. C.; Wynblatt, P. The chemisorption of CO and NO on Rh(110). *Surf. Sci.* **1980**, *97*, 346−362.

(54) Root, T. W.; Schmidt, L. D.; Fisher, G. B. Adsorption and reaction of nitric oxide and oxygen on Rh(111). *Surf. Sci.* **1983**, *134*, 30−45.

(55) Mukadi, L. S.; Hayes, R. E. Modelling the three-way catalytic converter with mechanistic kinetics using the Newton−Krylov method on a parallel computer. *Comput. Chem. Eng.* **2002**, *26*, 439−455.

(56) U.S. Census Bureau; *2007−2011 American Community Survey, 2011 American Community Survey 5-Year Estimate, travel time to work by zip code, table B08303*. http://factfinder2.census.gov (accessed on October 30, 2014).

(57) *U.S. diesel and hybrid passenger vehicle registration data (2010−13)*; Diesel Technology Forum: Frederick, MD, 2014. http://www.dieselforum.org/files/dmfile/DieselTechnologyForum-2014LightDutyTopTenLists.pdf (accessed on January 15, 2014).

(58) Garten, C. T. Nitrogen isotope composition of ammonium and nitrate in bulk precipitation and forest throughfall. *Int. J. Environ. Anal. Chem.* **1992**, *47*, 33−45.

(59) Geng, L.; Alexander, B.; Cole-Dai, J.; Steig, E. J.; Savarino, J.; Sofen, E. D.; Schauer, A. J. Nitrogen isotopes in ice core nitrate linked to anthropogenic acidity change. *Proc. Natl. Acad. Sci. U.S.A.* **2014**, *111*, 5808−5812.

(60) Burch, S. D.; Keyser, M. A.; Colucci, C. P.; Potter, T. F.; Benson, D. K.; Biel, J. P. *Applications and benefits of catalytic converter thermal management*. Technical paper no. 961134 for the Society of Automotive Engineers Fuels & Lubricants Spring Meeting: Dearborn, MI, 1996. DOI: 10.4271/961134.

(61) Laing, P. M. *Development of an alternator-powered electrically-heated catalyst system*. Technical paper no. 941042 for the Society of Automotive Engineers International Congress & Exposition: Detroit, MI, 1994. DOI: 10.4271/941042.

(62) Burk, P. L.; Hochmuth, J. K.; Anderson, D. R.; Sung, S.; Tauster, S. J.; Tolentino, C. O.; Rogalo, J.; Miles, G.; Niejako, M.; Punke, A.; Dahle, U. *Cold start hydrocarbon emissions control*. Technical paper no. 950410 for the Society of Automotive Engineers International Congress & Exposition: Detroit, MI, 1995. DOI: 10.4271/950410.